Earthquake Geotechnical Engineering for Protection and Development of Environment and Constructions – Silvestri & Moraci (Eds)
© 2019 Associazione Geotecnica Italiana, Rome, Italy, ISBN 978-0-367-14328-2

Liquefaction case histories after the 2016 megathrust Pedernales earthquake in Ecuador

X.F. Vera-Grunauer, S. Lopez-Zhindon, J. Ordoñez-Rendon & M.A. Chavez-Abril
Geoestudios S.A., Guayaquil, Ecuador

ABSTRACT: After the extensive damage that the 2016 Mw 7.8 Ecuador Earthquake produced, the early response of local and international organizations together with the continuous monitoring of private companies, allowed to collect valuable data of sites with geotechnical manifestations produced during the Earthquake. Particularly, liquefaction and its related effects were observed on numerous sites along the northwest and west coast of Ecuador. Many of these sites were studied and analyzed, some of them with various exploration techniques (e.g., shear wave velocity, Chinese dynamic cone penetration, cone penetration test, standard penetration test, and dilatometer tests). This document summarizes six cases of liquefaction that were heavily monitored, and whose results provide valuable information for liquefaction data.

1 INTRODUCTION

On the evening of April 16, 2016, an M_w7.8 earthquake struck northwestern Ecuador, leaving extensive damage throughout the Ecuadorian coast. Abundant geotechnical data was collected where liquefaction manifestations were observed. Exploration techniques included shear wave velocity (V_s), Chinese dynamic cone penetration (DPT), cone penetration tests with pore water measurement (CPTu), standard penetration tests (SPT), and dilatometer tests (DMT). This document presents the geotechnical characterization and the liquefaction evaluation of six well-documented sites.

Liquefaction surface manifestations included flow failure and lateral spreading in embankments, sand boils, and ejecta. Figure 1 shows the sites location and its distance to the epicenter. Due to the earthquake directivity (Ye 2016), most of the damage occurred towards the south of the epicenter. The geotechnical exploration in all the sites consisted of CPTu, SPT (with energy measurement through a pile driving analyzer device), and V_s tests, in addition to Chinese DPT and DMT tests at Site 1 (Port of Manta) and Site 3 (Briceño), respectively. The number of tests and the liquefaction manifestations occurred are listed in Table 1.

Site 1 (Port of Manta) is conformed of embankments that were constructed through hydraulic fills without adequate compaction. Particular interest arises in this site since both sand and gravel liquefaction was observed. Site 3 (Mejia Embankment) and Site 4 (Briceño Embankment) are road embankments that are part of the state road system. These sites are located in natural deposits of alluvial sands. The geological setting of Site 2 (Tarqui Neighborhood), Site 5 (Manta Overpass), and Site 6 (Mobil gas station) includes alluvial and colluvial deposits; however, in these sites, there has been an intense urban development of platforms construction for infrastructure. Thus, fill materials were encountered over the alluvial and colluvial deposits in these sites.

2 PEAK GROUND ACCELERATIONS (PGA)

Site 1, 2, 3, 5 and 6 were located at a close distance of a seismic station that recorded the earthquake. Site 1, 2, 5, and 6 are located at less than 5 km from AMNT Station (IG-EPN 2016), which has a V_{s30} of around 496 m/s, corresponding to a Soil Type C, according to the National

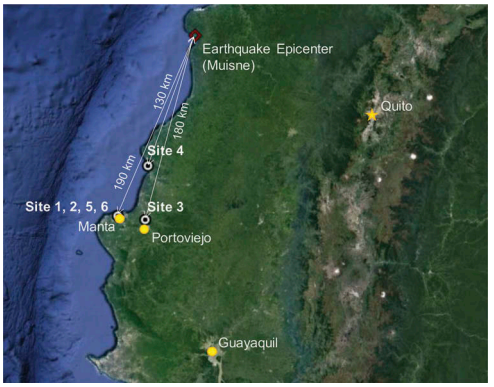

Figure 1. Location of the sites evaluated (Google Earth 2018).

Table 1. Tests, liquefaction manifestations and PGA adopted for the liquefaction evaluation for each site.

		Tests Performed						Liquefaction Manifestations				
Site		*SPT*	*CPTu*	*DMT*	*Chinese DPT*	*MASW + MAM*	*Cyclic TX*	*Ejecta*	*Sand Boils*	*Lateral Displ.*	*Settlement*	PGA (g)
Site 1: Port of Manta	Marginal Wharf	8	3	-	6	9	-	X	-	X	X	0.46(R)
	Breakwater	6	3	-	-	3	-	-	-	X	-	
	Yards	11	7	-	-	5	1	X	-	X	X	
Site 2: Tarqui Neighborhood		28	25	-	-	36	3	X	-	X	X	Various(S)
Site 3: Mejia Embankment		2	1	-	-	1	-	X	-	X	X	0.35(R)
Site 4: Briceno Embankment		6	15	4	-	2	-	X	X	X	X	0.40(E)
Site 5: Manta Traffic Overpass		4	-	-	-	-	-	X	-	-	X	0.35(S)
Site 6: Mobil Gas Station		2	-	-	-	-	-	X	-	-	X	0.35(S)

Note: (E) PGA estimated through ground motion prediction equations or external references
(R) Recorded PGA in a seismic station
(S) Obtained through a Site Response Analysis (SRA)

Earthquake Hazard Reduction Program (BSSC 2003) soil classification. In this station, the mean horizontal peak ground acceleration (PGA) from NS &WE components reached 0.46 g, which was adopted for Site 1. In the case of Site 2, 5 and 6, however, the PGA was obtained through total stress site response analyses (SRA) by propagating a deconvoluted AMNT seismic record (see Vera-Grunauer et al. 2017). Site 3 is located at <10 km distance from APO1 Station in the city of Portoviejo. This site qualifies as Type D, according to BSSC (2003), and the PGA reached 0.35 g. Since the site of the seismic station did not show liquefaction manifestations, it is believed that the PGA recorded is representative for the analysis at Mejia Bridge. In addition, by comparing the PGA recorded in this station with the predicted through different ground-motion prediction equations (GMPEs) (Abrahamson et al. (2016), Zhao et al. (2006), Ghofrani and Atkinson (2014), Montalva et al. (2017)), as presented in Beuval et al. (2017), the PGA fits within the limits of the mean plus one standard deviation of the GMPEs. Thus, the PGA value

of 0.35 g was adopted for the analysis. For Site 4 there is not a seismic station in a distance closer to 40 km. Thus, the PGA was obtained according to the GMPEs presented in Beuval et al. (2017) for a site with V_{s30}=400 m/s, which resulted in a mean value of 0.4 g. This PGA is consistent with the considered by Smith & Wissman (2018), who elaborated a detailed study of the embankment stability during the earthquake, adopting a PGA of 0.38 g.

3 SITES GENERAL DESCRIPTION

The following general descriptions depict overall geotechnical aspects of the locations mentioned in Table 1. Relevant results and comparisons regarding the cyclic behavior of the affected site ground conditions are presented in Section 4.

3.1 *Manta Port*

The Port of Manta, located in the city that bears its name, suffered large damage during the earthquake. Numerous liquefaction manifestations were observed: sand ejecta, settlement, and lateral spreading, affecting most of its infrastructure; which included the Marginal Wharf, the Breakwater, and to a significant extent the parking lot location, named as Yard 500. Figure 2 shows an aerial view of the port and the liquefaction manifestations. Detailed measurements of the cracks were recorded days after the earthquake by the GEER team (Nikolaou et al. 2016) and an extensive geotechnical exploration was performed in the following weeks (see Table 1). Further description of 3 key locations at Manta Port regarding liquefaction damage are mentioned in this section, relating to Manta Port´s: Marginal Wharf, the Breakwater and the Yard 500.

3.1.1 *Marginal Wharf (Manta Port)*

The Marginal Wharf suffered lateral and vertical deformations that ranged up to 18 and 46 cm, respectively (Nikolaou et al. 2016). The soils that conform the embankment classified as GM, GP, and GW per ASTM D-2487 (ASTM 2011) and materials of silt and fine sand were ejected through the cracks. Although different tests were performed in the embankment, as is shown in Table 1, only the V_s and the Chinese DPT tests provided solid and consistent information for the liquefaction evaluation. While the CPTu and SPT showed high variability, reporting the

Figure 2. (a) Port of Manta plan view (b) cracks observed in the Breakwater, (c) cracks and ejecta observed in Yard 500, (d) and (e) cracks and vertical displacement observed in the Marginal Wharf.

refusal at different shallow depths (Lopez et al. 2018). Through these tests, a layer of gravel-sand-silt mixtures and poorly graded gravel with low shear resistance was located between 3 to 11 m depth. The V_s values in this layer ranged from 100 to 150 m/s, with a media of 125 m/s, and the blowcount number, N'_{120}, of the Chinese DPT reported average values of 5 to 17 blows with an average of 7 blows in the layer that is believed to have liquefied. Liquefaction analyses were performed in the Chinese DPT and V_s tests, following the procedures presented in Cao et al. (2013) and a modified procedure of Andrus & Stokoe (2000).

Cao et al. (2013) present a probabilistic liquefaction evaluation in natural gravel deposits after the 2013 Wenchuan earthquake in China. The empirical formulation developed through the liquefaction analysis in their data set was used for the present analysis. Although the Manta Port and the gravel deposits evaluated in Cao et al. (2013) have different depositional environments, the grain size distribution and the gravel content are similar to the ones in this study.

Andrus & Stokoe (2000) present a liquefaction procedure based on the V_s values. While the authors' data covers soils that range from silty sand to gravels, with 36 case cases of gravelly soil out of the 225 total cases, the combination of the different soils in their formulation can bias the results, and the CRR curve recommended. Consequently, Chang et al. (2014 and 2016) developed a series of laboratory tests in different gravelly soils to determine the CRR curve. Through their results, the CRR curve of Andrus & Stokoe (2000) was modified to fit better to the liquefaction observed. The authors suggested that the procedure proposed by Andrus & Stokoe (2000) multiplying the CRR curve by a factor of 1.75 results in a fairly correct approximation for preliminary liquefaction potential evaluation. Thus, considering the significant variation in the GC in the soil of the embankment, the procedure of Andrus & Stokoe (2000) multiplying the CRR curve by a factor of 1.75 was adopted for the liquefaction evaluation.

In Section 4 results and comments are presented on the Cao et al. (2013) procedure for the DPT, as well as the results of the liquefaction analysis through the 1.75 scaled Andrus & Stokoe (2000).

3.1.2 *Breakwater (Manta Port)*

The Breakwater of the Port of Manta is a 16 m height embankment, whose body is composed of a rockfill of 5 to 6 tons rocks over sand materials that constitute the seabed (see Figure 3). During the construction the rocks were deposited to conform the embankment, without any improvement or replacement of the soil of foundation; thus a 2 m layer of liquefiable sand was confined at the bottom of the embankment. The lowest $(N_1)_{60}$ values reported in this layer is about 24, and the liquefaction evaluation through the Boulanger & Idriss (2014) procedure showed a high liquefaction potential, which was reflected in the deformations observed in the embankment after the earthquake as is shown in Figure 2 (b).

The lateral displacement ranged from 20 to 60 cm through different zones of the embankment. Pseudo-static analyses were performed, considering the residual undrained resistance (S_r) of the sand layer in the bottom of the embankment by correlations to the $(N_1)_{60}$, as proposed by Weber (2015). The S_r values ranged from 21 to 33 kPa considering the different confining pressures along

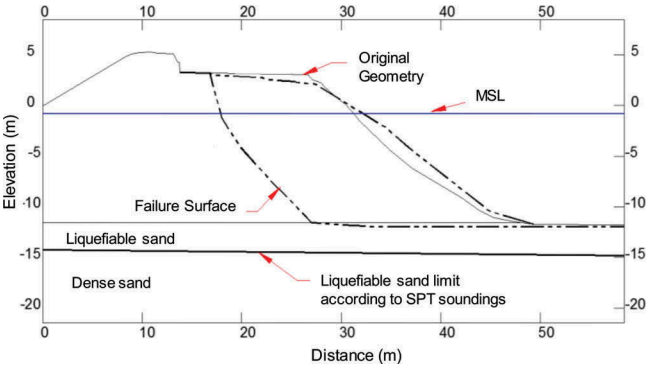

Figure 3. Geometry of the Breakwater before and after the earthquake.

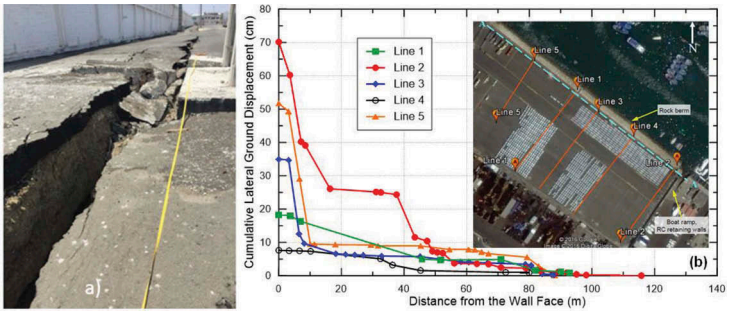

Figure 4. Yard 500 (a) settlements and pavement cracking (b) Measurements of the cumulative lateral displacement along five alignments in Yard 500 (Nikolaou et al. 2016).

the slopes in the embankment. The analysis showed that the failure plane intercepted the sand layer; however, the significantly low Factors of Safety did not reflect the relatively slight damage observed through the embankment. Due to the confining pressure and the blowcount number, the sand layer showed a dilative behavior, according to Olson & Stark (2013), limiting the flow failure potential, which could have been expected for the embankment geometry and its soil conditions. See Section 4 for further liquefaction analyses results within this studied site.

The displacement in the embankment was verified through the Bray & Macedo (2017) simplified procedure to estimate the seismic slope displacement for subduction zone earthquakes. The authors developed a semiempirical procedure that captures the main parameters that influence the behavior of the earth system during the earthquake (yield coefficient, k_y, initial fundamental period T_s, and the ground motion's spectral acceleration at a degraded period of the slope). Although this method is based on data of no-liquefiable soils, it can provide ranges and index on the displacements and damage expected in embankments. The estimated deformations obtained were in the range of 10 to 45 cm, which fit well with the observed range of displacements, validating the residual strength adopted for the pseudo-static analysis.

3.1.3 *Yard 500 (Manta Port)*

Within Manta Port, the parking lot location named as Yard 500 was heavily affected by liquefaction in terms of significant volumetric deformations (settlements) and to a lesser extent lateral deformation. The overlying pavement structure was significantly damaged, exhibiting settlements as large as 60 centimeters (see Figure 4a), and crack widths of up to 32 cm approximately. The soil profile is predominantly conformed of coarse sandy soils with a wide range of relative density. Loose sandy soils were present at shallow locations of approximately 3.0 meters below the ground surface, which confirmed the significant impact upon the area of Yard 500 due to liquefaction. A significant amount of sand ejecta was observed (Figure 2b) at the surface of the studied site. Settlements and lateral displacements were measured (see Figure 4b) at several locations of the studied site, where CPTu and SPT tests were performed, thus allowing a comparison between estimations and measured values. See Section 4 for the results of the analysis of this site regarding liquefaction evaluation and deformations through SPT and CPTu-based methodologies.

3.2 *Tarqui neighborhood*

The neighborhood of Tarqui was a densely populated and the main commercial zone of Manta, where 70% of the infrastructure was destroyed after the earthquake according to the Ministries of Urban Development & Housing (MIDUVI). Some of the liquefaction manifestations are shown in Figure 5, where the damage observed in Site 5 and 6 are also included. Extensive geotechnical exploration was developed in this area as is shown in Figure 6, covering the diverse deposits and areas of a different magnitude of damage. Through this exploration, characteristic soil columns and shear wave velocity profiles were defined in order to perform site response analysis (SRA). The SRA defined zones of similar dynamic behavior as shown in Figure 6 (b) and an accurate peak ground acceleration was obtained for the liquefaction analysis, through total stress SRAs.

Figure 5. Liquefaction manifestations and liquefaction-induced damage observed at Site 2 (Tarqui neighborhood) and Site 5 (Manta Traffic Overpass).

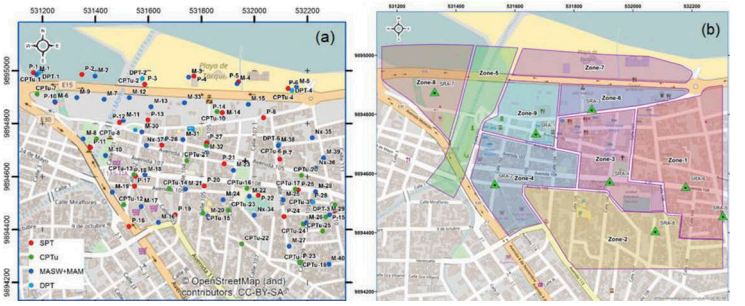

Figure 6. (a) Subsurface investigation and (b) Zonation and SRAs location in the Tarqui study area (Vera-Grunauer et al. 2017).

Liquefaction was evaluated in SPT and CPTu tests. Depicted results are shown at Section 4 for this studied site, which show that the semi-empirical liquefaction triggering methodologies for both the SPT and CPTu tests generally match well with the observations.

3.3 *Mejia embankment*

This section presents the liquefaction and lateral displacement evaluation of the Mejia Bridge Embankment, which suffered a catastrophic failure during the earthquake. The Mejia bridge is located about 8 km north of the city of Portoviejo and is part of the state roads system of Ecuador. The failure of its approach impacted local connectivity, ability to quickly receive supplies and the access of emergency vehicles to some of the most affected areas.

An aerial view of the failure at the Mejia Bridge site is shown in Figure 7 (a) with sketched markups of the observed movement of the embankment along assumed failure planes at the left side of the embankment (Nikolaou et al. 2016). The failure planes appear to be either along the interface between the embankment and the foundation soils (planar surface) or through the foundation soils. The latter, indicative of a circular surface failure may be due to

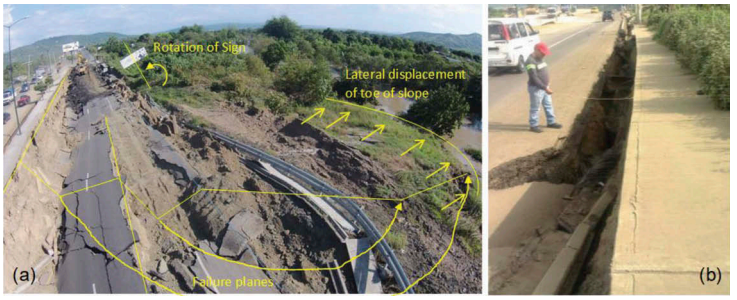

Figure 7. Mejia Bridge, (a) aerial view of the left side embankment failure with assumed movement and failure modes marked with yellow and (b) right side view of the embankment after the earthquake.

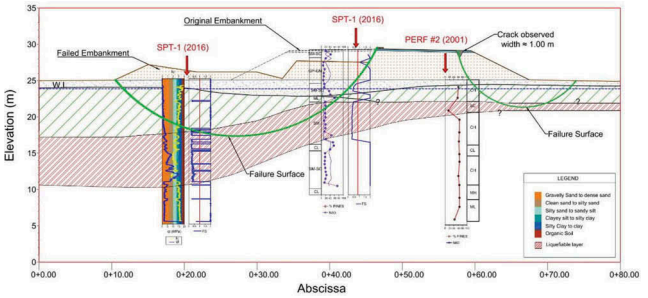

Figure 8. Mejia embankment schematic cross section and exhibited failure mechanisms.

liquefaction-induced softening that allowed the reduced-strength soil to shear in the earthquake. The embankment´s left side exhibited lateral displacements around 4-5 meters approximately. For the right side (see Figure 7b), although the horizontal displacements reached 1.0 m, the embankment did not show a deep-seated catastrophic failure as on the other side.

Before the construction of the bridge, an SPT test had been performed in the current location of the approach, and after the earthquake, one SPT and one CPTu tests were performed at the top and the bottom of the embankment, respectively. Figure 8 presents the location of the geotechnical exploration, the geometry of the original and failed embankment, and the results of the liquefaction evaluation following the procedure of Boulanger & Idriss (2014). Through the geotechnical exploration, a layer of loose sand was identified under the embankment, which varies in thickness, reaching 6 to 7 m in the left side of the embankment and decreasing to 1 to 1.5 m in the right side. The variation of the liquefiable layer is directly related to the different degree of damage observed in the embankment. The thicker and deeper liquefiable layer in the left side met the conditions for a flow failure, while the decrease in its thickness in the right side limited the displacements observed in the embankment according to Olson & Stark (2003) (see Section 4).

Limit equilibrium analyses in static and pseudo-static conditions were performed to evaluate the stability in both sides of the embankment as shown in Figure 9. For the pseudo-static condition, the undrained residual strength of the liquefiable layer was adopted according to the procedures of Olson & Stark (2002), Kramer (2015), and Weber (2015). Table 2 the Factors of Safety (FS) obtained. Although in static conditions the embankment presents adequate stability conditions, in the pseudo-static analysis the FS in the left side is lower to 1.

Simplified approaches were employed to estimate the existing lateral deformation at the left side of the embankment. Available cone penetration test (CPTu) data was used with a free face condition of L/H=3 (see Section 4). In addition, the method developed by Bray & Macedo (2017) for estimating seismically induced lateral displacements in slopes at subduction

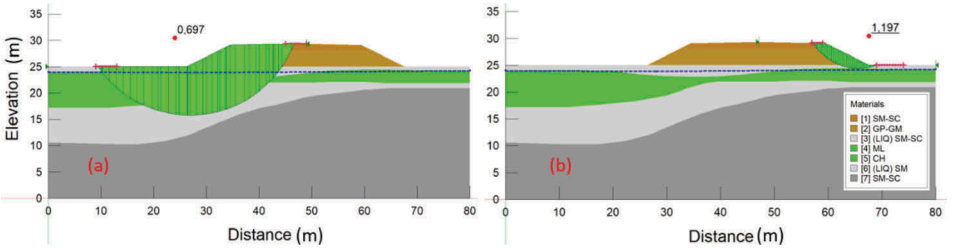

Figure 9. Results of the pseudo-static limit equilibrium analyses for (a) left side of the embankment and (b) right side of the embankment.

Table 2. Factors of safety for limit equilibrium analysis of the Mejia embankment.

Side	Factor of Safety	
	Static	Pseudo-Static
Left	2.78	0.70
Right	1.89	1.20

zones was used. Although this method is not conceived for evaluating lateral displacements in liquefiable soils, it can provide ranges on the displacements and damage expected in embankments. In this case, a horizontal deformation of approximately 3.0 meters was estimated, thus showing an acceptable estimate of potential horizontal soil displacements. Results regarding proxies of liquefaction potential in terms of cone resistance and cyclic stress mobility are shown in Section 4.

3.4 *Briceño bridge-embankment*

The embankment of the approach to Briceño bridge, located approximately at 7 km distance from Canoa city, was subjected to a geotechnical site investigation as means to study the performance of ground improvement technique adopted at the referred location. The embankment of the mentioned bridge was constructed over an improved soil via Rammed Aggregate Piers (RAPs). A shallow and soft layer of clayey material overlaid a loose sandy layer with some intercalations of finer soils. Although large liquefaction was observed in the adjacent areas to the embankment through sand boils and sand ejecta as shown in Figure 10, the embankment showed an outstanding performance against undrained cyclic soil behavior during the Muisne earthquake of 2016 when comparing the observed damage between Mejia

Figure 10. Liquefaction evidence through sand boils and sand ejecta observed in a free-field area adjacent to the embankment (Nikolaou et al. 2016).

Figure 11. Embankment seismic performance (a) Mejia embankment (b) Briceño embankment.

Figure 12. (a) Damage observed in the slab of Manta traffic overpass due to differential settlement and (b) Manta´s Mobil gas station after earthquake events of Muisne 2016.

embankment and Briceño´s case, presented above. Figure 11 depicts the damaged exhibited in both Mejia and Briceño embankments, showing the significant difference in seismic performance between improved a non-improved soil foundation underneath the mentioned embankments. It should be noted that in terms of seismic ground excitation, and geotechnical soil conditions, the Briceño embankment should have been prone to significant damage, provided that no soil improvement techniques (gravel columns) were employed.

3.5 *Manta traffic overpass and mobil gas station*

Site 5 (Traffic Overpass) and Site 6 (Mobil Gas Station) are closely located at the north-west of Tarqui Neighborhood, at Manta city (see Section 3.2). The traffic overpass suffered significant deformations and damage due to the earthquake, evidencing large settlements of approximately up to 30 cm. A shallow sandy layer of a thickness as large as 5 meters, overlies a medium dense sand stratum that is present up to 12 meters below the ground surface and beneath this medium dense layer a weathered rock matrix was identified. Figure 12 shows the existing differential settlement, which heavily damaged the slab at the base of the traffic overpass.

Manta´s Mobil gas station, which is located close to the seashore, suffered substantial damage as can be seen from Figure 12. A 3-meter-thick sandy layer of loose sand was underlying a medium dense fill material at the gas station location, evidencing the cause of surface damage due to the mentioned loose layer of mostly silty sands and poorly graded sands. In Section 4 results regarding liquefaction potential and measured and estimated deformations are presented for these sites.

4 RESULTS AND COMPARISONS

This section summarizes the liquefaction triggering evaluation, the liquefaction-induced settlements, and lateral displacement for the 6 sites described above. The lateral displacement and settlements estimated were quantitatively compared with the field measurements, where available. Liquefaction triggering evaluation was conducted using the Boulanger & Idriss (2014) and the Cetin et al. (2018) methodologies for the SPT, and the Boulanger & Idriss (2014) and Robertson (2009) for the CPTu. The SPT-based settlements were estimated through the Idriss & Boulanger (2008) and the Cetin et al. (2009) procedures for the author's respective triggering methodology; while for the CPTu-based estimations, the Idriss & Boulanger (2008) and the Robertson (2009) methodologies were considered. The lateral displacement was evaluated as proposed by Youd et al. (2002) and Zhang et al. (2004) for the SPT and CPTU tests, respectively. In the case of gravelly soils, the liquefaction triggering was evaluated through the Cao et al. (2013) and the modified Andrus & Stokoe (2000) procedures for the Chinese DPT and the V_s tests, respectively. In order to evaluate and compare the level of damage, index parameters were estimated through the Liquefaction Potential Index (LPI) (Iwasaki et al. 1978) and the Liquefaction Severity Number (LSN) (van Ballegoy et al. 2014). In addition, the upper non-liquefiable layer and the thickness of the liquefiable layer have been estimated, which can be contrasted with the Ishihara (1985) methodology for the evaluation of the expected liquefaction-induced damage.

In Tables 3 and 4 a summary of the SPT and CPTu boreholes analyzed is presented, respectively. For both tests, the boreholes of the Marginal Wharf are excluded. It can be seen in Table 3 that all sites classify as SM, SP, or SP-SM with an average fines content of 16%, while in Table 4 the I_c value ranges from 1.9 to 2.6. The LPI and LSN indicate the expected level of damage, which can be contrasted with those observed during the visits at the sites. While both, LPI and LSN indicate a certain degree of damage, the LSN indicates Minor to Non-damage in the SPT and CPTu tests of sites 1, 3 and 4; and Mayor in sites 5 and 6. Given the large lateral displacement and the significant sand ejecta observed for Sites 1, 3 and 4, the

Table 3 . Summary of the SPT-based liquefaction evidence compared to the liquefaction-induced damage prediction through the LPI and LSN index parameters.

						Estimations: Idriss & Boulanger (2014) / Cetin et al. (2018)													
Site	**PGA (g)**	**Liquefaction free field evidence**	**Boring**	**USCS**	**FC (%)**	**$N1_{60CS}$**		**LDI (m)**		**$S_{v\text{-}1D\ (m)}$**		**LPI** Iwasaki et al. (1978)		**LSN** van Ballegooy et al. (2014)		**Upper non liq. layer (m)**		**Cumulative thickness of liq. (m)**	
Site 1: Manta Yard 500	0.5	Sand ejecta, small to large cracks in parking area. Differential settlements and horizontal deformations	P2	SM	43	15	13	0.71	0.81	0.07	0.05	Moderate		Minor		2.9		2.3	
			P3	SM	15	15	14	0.61	0.47	0.06	0.03	Moderate		Minor	Little to non	4.9		2.2	
			P4	SP-SM, SM	23	17	16	0.75	0.74	0.08	0.05	Moderate		Minor	Minor	3.0		3.2	
			P5	SP-SM, SM	8	17	18	0.48	0.36	0.05	0.03	Moderate		Minor	Little to non	3.0		2.0	
			P6	SM, SP-SM	10	8	7	1.72	1.91	0.16	0.10	High		Moderate to sev.	Moderate	2.8		3.5	
			P8	SP-SM	8	18	18	0.72	0.58	0.08	0.05	Moderate		Minor	Little to non	3.2	3.5	3.5	3.2
Site 1: Manta Breakwater	0.5	Small to medium cracks. Large deformations. Rockfill lost	PT-38	SM-SP	8	24	28	0.09	0.15	0.02	0.00	Low	Low	Little to non	Little to non	15.7	15.7	0.6	3.2
Site 1: Manta Marginal Wharf		Lateral and vertical deformations, evidence of sand ejecta through cracks over the embankment	P-18	SP-SM, SM	11	15	14	-	-	-	-	-	-	-	-	-	-	-	-
			P-26	SM, GP-GM	12	23	22	-	-	-	-	-	-	-	-	-	-	-	-
			B-137	GP, GM-GP	5	8	8	-	-	-	-	-	-	-	-	-	-	-	-
			P-28	SM	15	16	15	-	-	-	-	-	-	-	-	-	-	-	-
Site 3: Mejía embankment	0.4	Embankment failure, severe lateral displacement 4 - 5 m	P1	SM	21	15	12	1.78	0.55	0.18	0.05	High		Moderate	Little to non	5.4		6.3	
Site 4: Briceño road embankment	0.40	Sand ejecta, sand volcanos and small cracks at the side of the road	P7	SM	18	17	15	0.24	0.28	0.03	0.02	Low	Moderate	Little to non		3.5		1.2	
			P8	SM	18	11	8	0.51	0.74	0.04	0.04	Moderate		Minor	Little to non	3.3		1.2	
			P9	SM, SP-SM	14	9	7	1.10	1.50	0.09	0.07	Moderate		Moderate	Minor	2.7		2.3	
			P10	SM	20	9	6	0.67	0.95	0.05	0.04	Moderate		Minor		3.5		1.4	
			P11	SM	14	9	7	0.78	1.06	0.07	0.05	Moderate		Minor		3.5		1.7	
Site 5: Manta overpass	0.4	Settlements from 5 to 30 cm around foundation. Sand ejecta	P3	SP-SM	10	20	20	0.85	0.58	0.13	0.04	Moderate		Minor	Little to non	5.5		5.5	
			P4	SP-SM	10	14	13	2.27	1.68	0.25	0.11	High		Mayor	Minor	3.5		7.5	
			P5	SP-SM	10	12	11	2.84	1.76	0.26	0.11	High		Mayor	Minor	3.5		7.5	
			P6	SP-SM	10	14	14	2.49	1.74	0.26	0.11	High		Mayor	Minor	3.5		8.5	
Site 6: Mobil gas station	0.4	Small cracks ≈ 5 cm and settlements up to ≈ 10 cm. Sand ejecta	P1	SM	29	10	6	0.10	0.10	0.01	0.01	Low		Little to non		2.3		0.2	
			P2	SM, SP-SM	12	9	7	0.00	0.00	0.04	0.03	Low	Moderate	Minor		2.0		0.9	

Table 4 . Summary of the CPT-based liquefaction evidence compared to the liquefaction-induced damage prediction through the LPI and LSN index parameters.

				Estimations: Robertson (2009) / Idriss & Boulanger (2014)											
Site	**PGA (g)**	**Liquefaction free field evidence**	**CPTu log**	**Ic**	**q_{1ncs}**		**LD (m)**	**$S_{v\text{-}1D}$ (m)**		**LPI** Iwasaki et al. (1978)		**LSN** van Ballegooy et al. (2014)		**Upper non liq. layer (m)**	**Cumulative thickness of liq. (m)**
Site 1: Manta Yard 500	0.46	Sand ejecta, small to large cracks in parking area. Differential settlements and horizontal deformations	1	2.6	102	103	2.20	0.24	0.19	Very high		Moderate	Moderate	4.5	4
			2	2.4	82	91	1.15	0.23	0.16	Very high		Minor	Minor	1.5	8.8
			4	2.3	86	93	3.45	0.27	0.20	Very high		Moderate	Moderate	5	2.9
			5	2.4	85	88	0.58	0.18	0.12	High	Very high	Little to non	Little to non	1.8	8.8
			6	2.3	90	100	1.55	0.25	0.19	Very high		Moderate	Moderate	4.5	3.5
Site 1: Manta Marginal Wharf		Lateral and vertical deformations, sand ejecta through cracks over the embankment	16	2.2	131	135	-	-	-	-	-	-	-	-	-
			17	2.2	117	112	-	-	-	-	-	-	-	-	-
			18	2.0	99	110	-	-	-	-	-	-	-	-	-
Site 3: Mejía embankment	0.32	Embankment failure, severe lateral displacement 4 - 5 m	1	2.1	92	110	5.80	0.2	0.2	Very high		Minor		4	3
Site 4: Briceño road embankment	0.4	Sand ejecta, sand volcanos and small cracks at the side of the road	10	1.9	122	108	0.28	0.02	0.01	High	Low	Little to non		-	-
			11	2.1	105	97	0.91	0.04	0.05	Very high	High	Minor		1.0	2.5
			12	2.3	85	86	0.34	0.02	0.01	High	Low	Little to non		-	-
			13	2.1	90	86	1.28	0.06	0.07	Very high	High	Moderate		0.9	3.2
			14	2.0	87	92	1.48	0.08	0.08	Very high	High	Moderate to severe		1.9	3.2
			15	2.1	98	96	0.85	0.04	0.04	Very high	High	Minor	Little to non	-	-
			16	2.1	96	107	0.78	0.04	0.04	High		Moderate	Minor	0.5	2.9
			7	2.1	88	87	0.62	0.03	0.03	Very high	Low	Minor	Little to non	0.6	2.8
			8	2.2	75	92	0.88	0.04	0.05	High		Moderate to severe	Moderate	-	-
			9	2.0	98	97	1.10	0.06	0.07	Very high	High	Moderate to severe		0.8	2.6
			2	2.3	84	87	1.12	0.04	0.05	High		Moderate		-	-
			3	2.0	92	108	0.77	0.05	0.06	High		Moderate		1.0	2.4
			4	2.2	68	79	0.81	0.04	0.04	High		Moderate	Minor	-	-
			5	2.3	59	76	1.15	0.05	0.05	Very high	High	Moderate		0.5	3.1
			1	2.2	103	104	1.05	0	0.1	High		Minor		0.9	4.5

LPI yields better qualitative descriptions on the damage after the 2016 Muisne earthquake for these sites. While in Sites 5 and 6, where settlements were the main liquefaction-induced effect, the LSN yields better predictions. Since the LSN is based on volumetric strains empirical equations, this index parameter better predicts settlement related liquefaction-damage. Consequently, for the sites that were subjected to lateral deformations, the LSN may not correctly predict the damage magnitude.

4.1 *Liquefaction evaluation*

Figures 13(a) and 13(b) present the liquefaction triggering evaluation for the SPT and CPTu, respectively. The deterministic triggering curves were considered, which correspond to liquefaction probability of 15% and 50% for the Boulanger & Idriss (2014) and the Cetin et al. (2018), respectively. The CPT-based approach proposed by Robertson et al. (2009) corresponds to a liquefaction probability of 35%, meaning that it is slightly on the conservative side. Site 2 has also been included, in which non-liquefaction data was also identified and is represented with empty symbols. For both, the SPT and CPT tests, the two methodologies correctly predict the liquefaction potential for most of the boreholes evaluated. The Boulanger & Idriss (2014) triggering method yields closer predictions to the field observations, while the Cetin et al. (2018) method seem to overestimate the liquefaction potential for the SPT. Similarly, the Robertson et al. (2009) method for the CPTu evaluations yields higher CSR values, which can overpredict the liquefaction potential.

For Site 1, the points of the liquefaction evaluation of the Breakwater and the gravelly soils of Marginal Wharf are presented in partially filled symbols. For the Breakwater, the Boulanger and Idriss (2014) method correctly predicts the liquefaction potential; while, the Cetin et al. (2018) falls in the non-liquefiable zone, close to the deterministic triggering line. For the Marginal Wharf, there was a lack of reliability in the execution of the SPT and CPTu tests in gravelly soils, since various of the tests performed did not reach the liquefiable layer depth. Therefore, only the CPTu

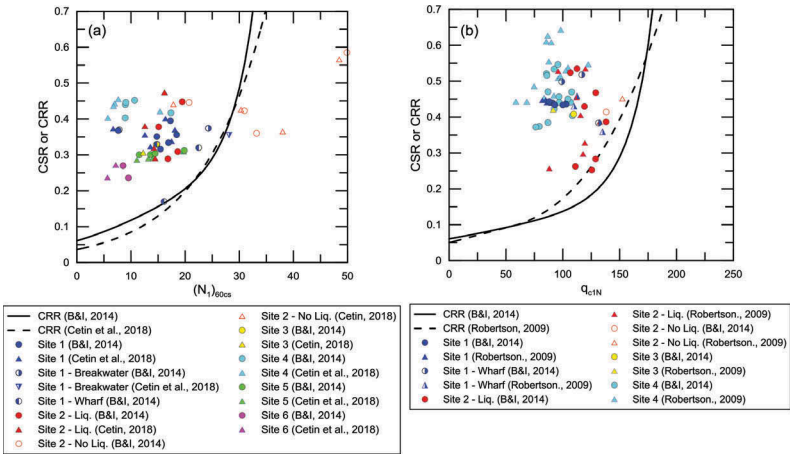

Figure 13. (a) CSR vs. N-values corrected for overburden and expressed in terms of equivalent clean sand $(N_1)_{60cs}$ and (b) CSR vs. qc-values corrected for overburden, and expressed in terms of an equivalent clean sand, q_{c1Ncs}.

and SPT tests that were able to advance through the gravels and to partially obtain the resistance of the liquefiable layer are plotted. Although, for both, the SPT and CPTu evaluations, the methodologies considered predict liquefaction, the blowcount and tip resistance measured is not uniform and do not represent the whole thickness of liquefiable layer as the Chinese DPT and V_s tests. The liquefaction triggering evaluation through these tests is presented in Figure 15.

For Site 3 (Mejia Embankment) a static shear stress value is applied in the analysis to contemplate the embankment influence on the liquefiable materials, which increases the CSR value. In the case of Site 4 (Briceño), the higher values of CSR observed are due to the higher PGA estimated for this site, which was closer to the epicenter.

Figure 14 (a) presents the comparison of the liquefaction-induced settlements. While significant scatter within a factor of ± 2 of the measured settlement was observed for all the range of settlements of this study, the Cetin et al. (2018) yields closer estimations for the lower settlements (< 10 cm). For larger settlements, however, this methodology underpredicts the settlements. On the other hand, the methodologies of Idriss and Boulanger (2008) for the CPTu and SPT tests, and the Robertson (2009) for the CPTu were more consistent with field observations for larger settlements.

Figure 14 (b) presents the SPT and CPTu-based liquefaction-induced lateral displacement comparison for Yard 500 and the Breakwater at Site 1, and for Mejia Embankment in Site 3. The lateral displacement in Yard 500 followed the north-east direction, towards the rock berm in the limit of the yard to the sea (see Figures 2a and 4b). As shown in Figure 4b, Nikolaou et al. (2016) present the measurements of the cumulative lateral displacement starting from the rock berm along different perpendicular alignments, across the yard. The corresponding cumulative lateral spread displacement measurement of the location of the borehole evaluated to the nearest line was adopted for the comparisons. For the Breakwater, lateral displacements occurred in the inner part of the embankment, and for Mejia Embankment, the major displacement occurred on its left side. For lateral displacements less to 1.0 m, a poor agreement between estimated and measurements displacements is observed when considering the CPT-based analysis of Yard 500 by applying the method proposed by Zhang et al. (2004). Conversely, the SPT-based procedure proposed by Youd et al. (2002) yielded an acceptable agreement with the measured lateral deformations in this range. For larger displacements, however, like that occurred at Mejia Embankment, the Zhang et al. (2004) method yields better estimations to those occurred after the earthquake.

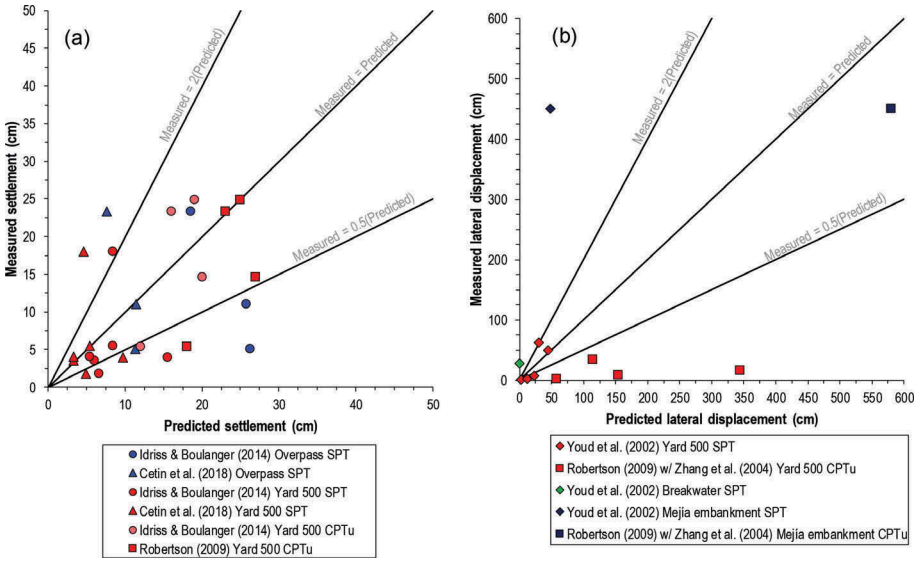

Figure 14. Comparison between measurements and estimations of the (a) liquefaction induced settlement and (b) liquefaction-induced lateral displacement in various sites.

4.2 *Liquefaction triggering evaluation in gravely soils*

Due to the limitations in the SPT and CPTu tests to correctly identify the gravelly soil's resistance along the Marginal Wharf as presented in Figure 13, the liquefaction triggering was also evaluated through the Chinese DPT and V_s tests. Figure 15 (a) presents the liquefaction evaluation results through the Cao et al. (2013) procedure for the Chinese DPT, and Figure 15 (b) presents the results of the liquefaction analysis through the 1.75 scaled Andrus & Stokoe (2000) procedure as recommended in Chang et al. (2014) for the V_s data. As can be seen in the figures, both analyses confirm the high liquefaction susceptibility in the gravel soils. However, the Cao et al. (2013) procedure showed more consistency with the observations, since two points of their data showed a lower liquefaction potential in zones of the Marginal Wharf where lower damage was observed.

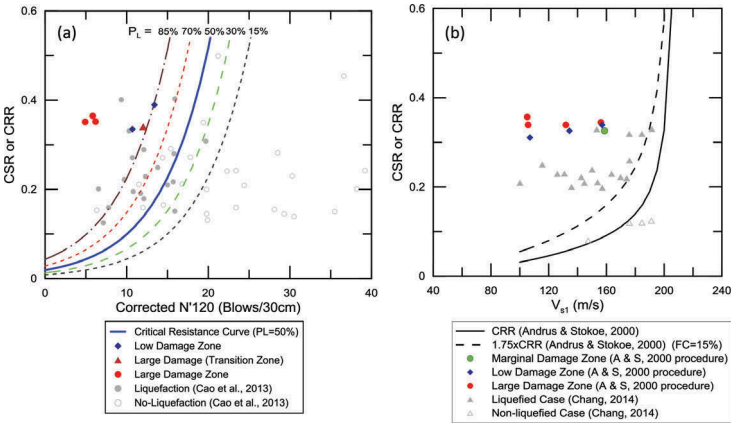

Figure 15. Liquefaction evaluation in gravelly soils of Site 1 (Marginal Wharf) for the (a) Chinese DPT through the Cao et al. (2013) and (b) V_s through the modified Andrus & Stokoe (2000) procedure.

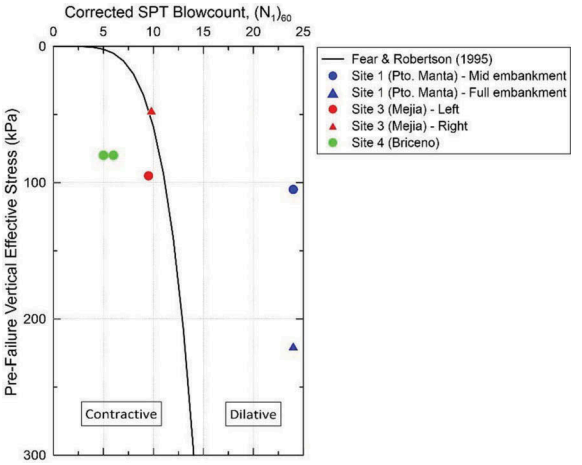

Figure 16. Flow liquefaction evaluation (Olson & Stark 2003).

4.3 *Flow liquefaction*

The flow liquefaction potential was evaluated for the embankments of Site 1, 3, and 4. Olson & Stark (2003) present a methodology to evaluate the potential for an embankment to undergo flow liquefaction. In their procedure, the authors recommend applying the Fear & Robertson (1995) method for a preliminary evaluation, which relies on the soil contractive or dilative behavior to define the flow potential. The behavior is assessed through its relative density, defined by the $(N_1)_{60}$ value, and through the confinement pressure at the liquefiable layer.

Figure 16 presents the evaluation for the sites described. In the case of the Breakwater at Site 1, due to the height of the embankment, two confining pressure were considered, one that represents the confining pressure of the whole embankment, and the other under the slopes of the embankment. It can be seen in Figure 16 that in both cases the points lay in the dilative behavior area, which implies that no flow liquefaction is likely to occur. In the case of the Mejia embankment of Site 2, the left side lies under the contractive behavior, being prone to undergo flow liquefaction, as it was observed during the earthquake. The right side, however, suffered limited deformation, which is consistent with the predictions of flow liquefaction, where according to Olson & Stark (2003), presents dilative behavior. For the case of Briceño, a comparison between the flow liquefaction potential and the embankment performance during the earthquake cannot be completed since the site was improved with a RAPs system. However, flow liquefaction was evaluated in two boreholes performed in free-field and corrected to the overburden confining pressure of the embankment. As shown in Figure 16, for both cases the combination of relative density and confinement of the liquefiable layer indicates the susceptibility of the embankment to flow liquefaction.

5 CONCLUSIONS

The 2016 Ecuador Earthquake left significant damage along the northwestern Ecuadorian coast. Numerous geotechnical damages were observed, including liquefaction manifestations in sands and gravelly soils. Six liquefaction cases that were thoroughly investigated through various exploration techniques have been characterized and analyzed, verifying the liquefaction susceptibility, flow liquefaction potential, and lateral displacement.

Damage index parameters, as the Liquefaction Potential Index (LPI) and the Liquefaction Se-verity Number (LSN) were evaluated and contrasted with the observations in the sites.

Results showed that the LPI better predicts the level of damage, particularly for the sites where large lateral displacements occurred. Since the LSN is based on volumetric strains empirical equations, this index parameter better predicts settlement related liquefaction-damage.

The results of the liquefaction triggering analyses validated the liquefaction susceptibility in gravelly soils through a modified Andrus & Stokoe (2000) procedure, as recommended in Chang et al. (2014), for the V_s data, and the Cao et al. (2013) procedure using DPT data, being the Cao et al. (2013) more consistent with that observed in the field. For sandy soils, the Boulanger & Idriss (2014) methodology showed the best approximations with field observations. This method is recommended for the liquefaction evaluation in sandy soils in this study area.

Various methodologies to evaluate the liquefaction-induced settlement and lateral displacement were evaluated. For the sites analyzed, the Cetin et al. (2018) methodology yields closer estimations for the lower magnitudes of settlements. For larger measured settlements, however, this methodology underpredicts the settlements, being the Idriss and Boulanger (2008) methodology for the CPTu and SPT tests, and the Robertson (2009) more consistent with the observations. Regarding lateral displacements, the methodology proposed by Youd et al. (2002) for the SPT tests yielded a better agreement with those measured for displacements less than 1.0 m.

Through the evaluation in three embankments that suffered various degree of damage, the Olson & Stark (2003) method correctly predicts the flow liquefaction potential. Given the magnitude of damage observed when flow liquefaction occurs, this method provides a simple and straightforward tool to evaluate the damage expected in embankments located in liquefiable soils.

The results from these cases histories can contribute to further cases and can add valuable data to the liquefaction evaluation in sandy and gravelly soils.

REFERENCES

Andrus, R.D., and K.H. Stokoe II. 2000. Liquefaction resistance of soils from shear-wave velocity. *Journal of Geotechnical and Geoenvironmental Engineering*. 126(11):1015–1025.

ASTM International (ASTM). 2011. D2487-11 Standard Practice for Classification of Soils for Engineering Purposes (Unified Soil Classification System). West Conshohocken, PA.

Beauval, C., J. Marinière, A. Laurendeau, J.-C. Singaucho, C. Viracucha, M.Vallée, E. Maufroy, D. Mercerat, H. Yepes, M. Ruiz. 2017. Comparison of observed ground-motion attenuation for the 16 April 2016 Mw7.8 Ecuador megathrust earthquake and its two largest after-shocks with existing ground-motion prediction equations. *Seismol. Res. Lett*. 88, no. 2A, 287–299.

Boulanger, R.W., and Idriss, I.M. 2014. CPT and SPT based liquefaction triggering procedures. *Center for Geotechnical Modeling*. UC Davis.

Cao, Z., Youd T., and Yuan X. 2013. Chinese dynamic penetration test for liquefaction evaluation in gravelly soils. *J. Geotechnical and Geoenv. Eng*. 139(8):1320–1333.

Cetin, K.O., Seed, R.B., Kayen, R.E., Moss, R.E.S., Bilge, H.T., Ilgac, M., Chowdhury, K. 2018. SPT-based probabilistic and deterministic assessment of seismic soil liquefaction triggering hazard, *Soil Dynamics Earthquake Engineering*. Manuscript Number SOILDYN_2017_506.

Cetin, K.O., Bilge, H.T., Wu, J., Kammerer, A.M., and Seed, R.B. 2009. Probabilistic models for the assessment of cyclically induced reconsolidation (volumetric) settlements. *J. Geotechnical and Geoenv. Eng*. 135(3):387–398.

Chang, W. J. 2016. Evaluation of Liquefaction Resistance for Gravelly Sands Using Gravel Content–Corrected Shear-Wave Velocity. *J. Geotechnical and Geoenv. Eng*. ASCE 142(5)

Idriss, I.M., and R.W. Boulanger. 2008. Soil Liquefaction During Earthquakes. *Earthquake Engineering Research Institute* MNO 12. Oakland, CA: Earthquake Engineering Research Institute.

Instituto Geofísico at the Escuela Politécnica Nacional, IG-EPN. 2016. Acelerógrafos, Publicado en Instrumentación, igepn.edu.ec/acelerografos, last accessed 7/1/16.

Ishihara, K. 1985. Stability of natural deposits during earthquakes. *Proceedings of the 11th International Conference on Soil Mechanics and Foundation Engineering*, San Francisco, California.

Iwasaki, T., Tokida, K., Tatsuko, F., & Yasuda, S. 1978. A practical method for assessing soil liquefaction potential based on case studies at various sites in Japan. *Proceedings of 2nd International Conference on Microzonation* pp. 885–896. San Francisco.

Kramer, S.L. and Wang, C.H. 2015. Empirical Model for Estimation of the Residual Strength of Liquefied Soil. *J. Geotechnical and Geoenv. Eng*. ASCE, 04015038 (15).

Lopez, S., Rollings, K., Vera, X., & Salvatierra, G. 2018. Gravelly Soil Liquefaction after the 2016 Ecuador Earthquake. *Proceedings of the Geotechnical Earthquake Engineering and Soil Dynamics V*.

Nikolaou, S., Vera-Grunauer, X., & Gilsanz, R., eds., 2016. GEER-ATC Earthquake Reconnaissance: April 16 2016, Muisne, Ecuador, Rep. GEER-049, co-authors: Alvarado, A., Alzamora, D., Antonaki, N., Arteta, C., Athanasopoulos, A., Bassal, P., Caicedo, A., Casares, B., Diaz, V., Diaz-Fanas, G., Gilsanz, R., González, O., Hernandez, L., Kishida, T., Kokkali, P., López, P., Luque, R., Lyvers, G. M., Maalouf, S., Mezher, J., Miranda, E., O'Rourke, T., O'Connor, F., Rodríguez, L.F., Rollins, K., Stavridis, A., Toulkeridis, T., Vaxevanis, N., Wood, C., Yepes, H., Yepez, Y. Available at geerassociation.org.

Olson, S. M., and Stark, T. D. 2002. Liquefied strength ratio from liquefaction flow failure case histories. *Canadian Geotechnical Journal*. 39, 629–647.

Olson, S. M., and Stark, T. D. 2003. Yield strength ratio and liquefaction analysis of slopes and embankments. *J. Geotechnical and Geoenv. Eng*. 10.1061/(ASCE)1090-0241(2003)129: 8,727–737.

Robertson, P.K., and C.E. Wride. 1998. Evaluating cyclic liquefaction potential using the cone penetration test. *Canadian Geotechnical Journal* 35(3):442–459.

Seed, H. B., and Idriss, I. M. 1971. Simplified procedure for evaluating soil liquefaction potential. *J. Soil Mech. and Found*. ASCE, 97(9),1249–1273.

Van Ballegooy, S., Malan, P., Lacrosse, V., Jacka, M. E., Cubrinovski, M., Bray, J. D., Cowan, H. 2014. Assessment of Liquefaction-Induced land damage for residential Christchurch. *Earthquake Spectra*, 30(1).

Vera-Grunauer, X., Lopez, S., Gonzalez, O., Davila, D., Nikolaou, S., Ordonez, J., Aviles, A., Anton, A. 2017. Case History: Observed Liquefaction and its Evaluation after the April 16, 2016, Mw7.8 Muisne, Pedernales Earthquake. *PBD II Earthquake Geotechnical Engineering*.

Weber, J.P. 2015. Engineering evaluation of post-liquefaction strength. Ph.D. diss., University of California, Berkeley.

Ye, L., Kanamori, H., Avouac, J., Li, L., Cheung, K., Lay, T. 2017. The 16 April 2016, MW 7.8 (MS 7.5) Ecuador earthquake: A quasi-repeat of the 1942 MS 7.5 earthquake and partial re-rupture of the 1906 MS 8.6 Colombia–Ecuador earthquake. *Earth and Planetary Science Letters*, Volume 458, 15 January 2017.

Youd, T.L., C.M. Hansen, and S.F. Bartlett. 2002. Revised multilinear regression equations for prediction of lateral spread displacement. *J. Geotechnical and Geoenv. Eng*. 128(2):1007–1017.

Zhang, G., P. Robertson, & R. Brachman. 2004. Estimating liquefaction-induced lateral displacements using the standard penetration test or cone penetration test. *J. Geotechnical and Geoenv. Eng*. 130 (8):861–871.